Published in "Journal of Physics: Condensed Matter 22(23): 235102, 2010"
which should be cited to refer to this work.

Molecular liquid under nanometre confinement: density profiles underlying oscillatory forces

Edith Perret[1], Kim Nygård[1], Dillip K Satapathy[2], Tobias E Balmer[3], Oliver Bunk[1], Manfred Heuberger[4] and J Friso van der Veen[1,3]

[1] Paul Scherrer Institut, 5232 Villigen PSI, Switzerland
[2] Université Fribourg, 1700 Fribourg, Switzerland
[3] ETH Zurich, 8093 Zurich, Switzerland
[4] EMPA, 9014 St Gallen, Switzerland

E-mail: friso.vanderveen@psi.ch

Abstract
Ultrathin (<12 nm) films of tetrakis(trimethyl)siloxysilane (TTMSS) have been confined by atomically flat mica membranes in the presence and absence of applied normal forces. When applying normal forces, discrete film thickness transitions occur, each involving the expulsion of TTMSS molecules. Using optical interferometry we have measured the step size associated with a film thickness transition (7.5 Å for compressed, 8.4 Å for equilibrated films) to be smaller than the molecular diameter of 9.0 Å. Layering transitions with a discrete step size are commonly regarded as evidence for strong layering of the liquid's molecules in planes parallel to the confining surfaces and it is assumed that the layer spacing equals the measured periodicity of the oscillatory force profile. Using x-ray reflectivity (XRR), which directly yields the liquid's density profile along the confinement direction, we show that the layer spacing (10–11 Å) proves to be on average significantly larger than both the step size of a layering transition and the molecular diameter. We observe at least one boundary layer of different electron density and periodicity than the layers away from the surfaces.

1. Introduction

Knowledge about the structure of confined liquids is of great importance both in technology and nature. The structure may directly affect the liquid's physical properties such as lubrication, viscosity and adhesion. Simulations of e.g. hard sphere or Lennard-Jones systems (Snook and Henderson 1978, Kjellander and Sarman 1991, Wang and Fichthorn 2000, Ayappa and Mishra 2007), suggest that the liquid's constituents start to order in discrete layers parallel to the confining walls. Surface force experiments, in which the normal forces between two approaching surfaces with intervening liquid are measured to be oscillatory, provide evidence for this layering effect (Horn and Israelachvili 1981, Christenson 1983, Klein and Kumacheva 1998). Namely, discrete transitions in the film thickness are observed, which are reminiscent of the expulsion of successive layers. However, surface force experiments, by their very nature, do not directly reveal the out-of-plane structure of the confined liquid. The common method of structure determination is x-ray diffraction, but applying this technique to confined molecular liquids is a challenging task; the quantity of liquid is minute and the container shape has to be accurately known. Up to now, periodic microcavity arrays (Nygård *et al* 2008) or the so-called x-ray surface force apparatus (Golan *et al* 2002) have been used for investigations of confinement-induced ordering phenomena in fluids. These experimental setups are rigid containers, designed for x-ray diffraction studies of colloids and emulsions in transmission (Diaz and van der Veen 2007, Diaz *et al* 2005, Nygård *et al* 2009, Satapathy *et al* 2009, 2008) or for examining the

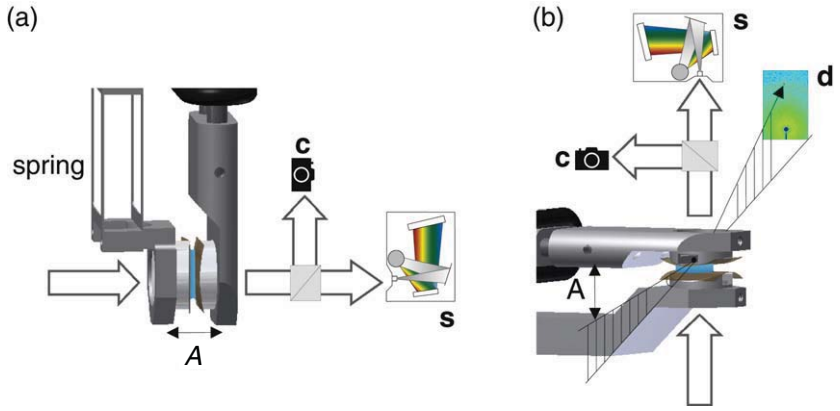

Figure 1. Schematic of the extended surface force apparatus with crossed-cylinder geometry. (a) Configuration featuring supported mica membranes glued onto spring-loaded silica discs (eSFA). White light passes through the interferometer and is analysed with a spectrometer s. The light is also directed into a CCD camera c to image the film in real time. (b) Configuration with free-standing mica membranes for XRR experiments. The specularly reflected x-rays are additionally recorded using a PILATUS 100 K detector (Kraft *et al* 2009) d. In both configurations a piezoelectric actuator is used to control the film thickness (indicated by A).

effect of shear (Idziak *et al* 1996a, 1996b, 1995). The width of the containers, which ranges from 100 nm to 1 μm in these studies, is too large for inducing confinement effects in molecular liquids. A recent structural investigation of a molecular liquid (OMCTS) between silicon surfaces at a few nanometre distance reported thickness quantization by a single molecular diameter (1 nm) under the application of a large normal force (Seeck *et al* 2002).

Here we present a novel confinement device (section 2), which enables us to determine the out-of-plane structure of molecular liquids under extreme nanometre confinement by synchrotron x-ray reflectivity (XRR) (Als-Nielsen and McMorrow 2001). X-ray reflectivity is the method of choice, since the perpendicular momentum transfer $q_\perp$ directly probes the laterally averaged electron density profiles along the confinement direction. Free-standing mica membranes are used as confining walls, with their atomically smooth surfaces being a prerequisite to resolve individual layers in the density profiles. X-ray reflectivity experiments were performed on confined tetrakis(trimethyl)siloxysilane (TTMSS) films of thicknesses below $<$12 nm. TTMSS is a silane oil and serves as a model liquid since it has a low vapour pressure and its molecules have a quasi-spherical shape similar to other non-polar liquids such as octamethylcyclotetrasiloxane (OMCTS), benzene, cyclohexane and toluene (Klein and Kumacheva 1998, Heuberger and Zäch 2003). These liquids have earlier been investigated by surface force experiments. They generally show pronounced oscillatory forces, with OMCTS being the first liquid for which such oscillatory forces have been measured (Horn and Israelachvili 1981, 1980).

In addition to XRR experiments, we have employed white light interferometry in order to determine the change in film thickness upon layer transition. These films, being confined by thin free-standing membranes, are essentially free of external forces under stationary conditions. We also confined TTMSS between supported mica membranes glued onto silica discs, enabling us to apply normal force. Under these conditions the step sizes of the thickness transitions differ from the ones measured for films confined between free-standing mica membranes. This discrepancy suggests the presence of film compression for measurements with supported mica. Moreover, the thickness transitions measured in the presence or absence of external forces, are generally smaller than the average layer spacing within the liquid as measured by XRR. We attribute this mainly to film thickness dependent changes in the layer spacings closest to the confining walls, which are different from the inner liquid layers (section 3).

2. Methods

An extended surface force apparatus (eSFA) (Balmer 2007, Heuberger 2001, Heuberger *et al* 2001) serves as confinement device. Two different configurations were used, one with supported mica membranes on a leaf spring mount for force measurements and one with free-standing mica membranes on a rigid mount for XRR experiments (figure 1).

Below, we first introduce the extended surface force apparatus (eSFA) and its adaptation to XRR experiments. Then we discuss our method for preparing confined films of large area and explain the film thickness measurements using white light interferometry. We conclude this section with details about the XRR experiments, which were performed at the coherent small angle x-ray scattering (cSAXS) beamline of the Paul Scherrer Institut.

2.1. Measurement of normal force

The eSFA (figure 1(a)) measures forces acting between two curved surfaces. Muscovite mica membranes of 2–6 μm thickness are covered with a silver layer of 40 nm thickness on their back side and glued onto silica cylinders. Both cylinders are mounted on sample holders in crossed geometry (90°). One of the sample holders is connected to an actuator (range 25 μm) which moves the cylinder with an accuracy of 50 pm. The other sample holder is connected to a double-leaf spring with spring constant $k = 946$ N m^{-1}. A cuvette surrounds these

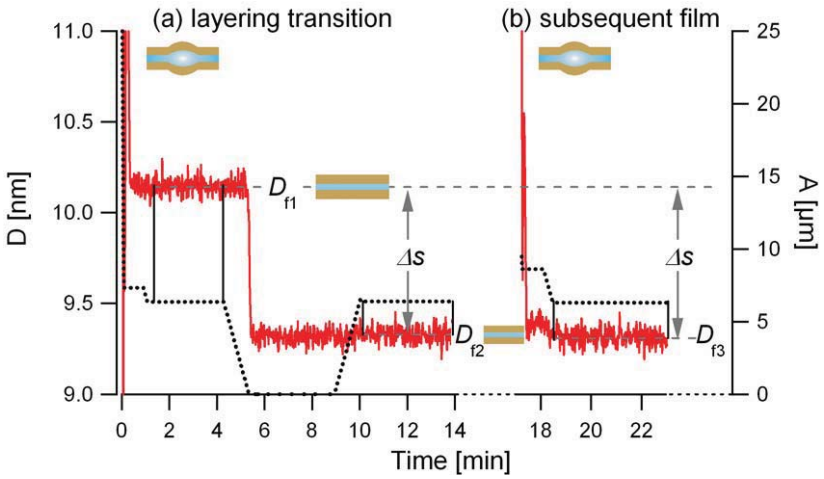

Figure 2. Example of recorded film thickness transitions. The film thickness D as measured via interference (red curve) and the actuator position A (dotted black curve) are plotted versus the time. (a) Determination of the change in film thickness $\Delta s = D_{f1} - D_{f2}$ during a layering transition from N to $N - 1$ layers. (b) Film of thickness D_{f3}, obtained from a liquid pocket of different size, as described in the text. Determination of Δs by comparing film thickness D_{f3} with a previous film thickness e.g. D_{f1}.

sample holders and is continuously flooded with dry nitrogen to keep the relative humidity low. The complete instrument is surrounded by an insulated enclosure in order to provide high thermal stability (Heuberger *et al* 2001).

The stack of silvered mica–liquid–mica layers functions as a high finesse Fabry–Perot interferometer (Born and Wolf 1980). White light from a Xe arc lamp is directed through the interferometer where it is reflected back and forth at each interface. The resulting interference spectrum is collected with an objective lens and directed to a CCD camera (c) and a spectrometer (s). This interferometry technique is employed to determine the optical distance between the silver mirrors, which can be used to determine the mica thickness and the film thickness D of the confined liquid (Born and Wolf 1980, Clarkson 1989, Heuberger 2001). The optical zero $D = 0$, when the mica sheets are in contact, has to be determined before filling with liquid. The optical zero can be offset due to irreversibly adsorbed water onto the hydrophilic mica surfaces after cleavage (Malani and Ayappa 2009, Christenson 1993, Balmer *et al* 2008). The normal surface forces are derived from Hooke's law: $F(D) = k(D - A)$, where A is the calibrated actuator position. Successive layering transitions in the liquid as a function of D are observed as force oscillations, from which the change in film thickness upon layering transition can be accurately determined. The measured step size is not affected by errors in the optical zero.

2.2. Free-standing mica membranes and film thickness transitions

The eSFA described in section 2.1 cannot be used for XRR, because the supporting silica discs and the silver layers would cause too much background x-ray scattering and would attenuate the x-ray beam. Therefore, thin free-standing mica membranes without silver coating are used for these experiments. Despite the absence of silver, which normally provides an optical resonator of high finesse, white light interferometry can still be employed, albeit at a slightly inferior single point resolution of 50 pm typically. The free-standing membranes are mounted as follows. Supporting metallic cylinders have rectangular areas cut out, which enable the incident and reflected x-ray beams to pass through without obstruction (figure 1(b)). Mica membranes of identical thickness are glued onto the cylinder edges leaving the central parts of the membranes unsupported. The cylinders are mounted in crossed axis geometry. The flexible spring is replaced by a rigid mount, since this setup is not used for normal force measurements because of the compliant mica membranes.

The pair of free-standing mica membranes precludes the application of a normal force as is possible for mica glued on silica discs. Nonetheless, the control of film thickness is still possible with limitations by using the hydrodynamic behaviour of the confined liquid between the curved membranes, as has been described by Balmer (2007) and is summarized below. A droplet of TTMSS is inserted between the free-standing mica membranes using a syringe. Upon fast approach of the mica membranes, liquid is trapped in a pocket, which slowly drains until a locally flat stable film with quantized thickness of a few nanometres and a lateral diameter of a few hundred micrometres is formed. In this configuration, the film thickness is determined by the liquid equilibrium structure. A small intrinsic pressure is exerted by the mica membranes at the edge of the contact zone. Layering transitions can be triggered by a dynamic decrease of A as shown in figure 2(a). The step size Δs is then simply determined by subtracting the film thicknesses D_{f1} and D_{f2}, i.e. before and after a layering transition from one another. However, the transient normal force in the film centre is usually too small to trigger a transition. In the latter case one uses individual approach cycles starting each time at a large mica distance, applying various approach speeds in a trial and error fashion. Liquid pockets of different sizes are created, which drain to form stabilized films of varying thickness. The flat films are

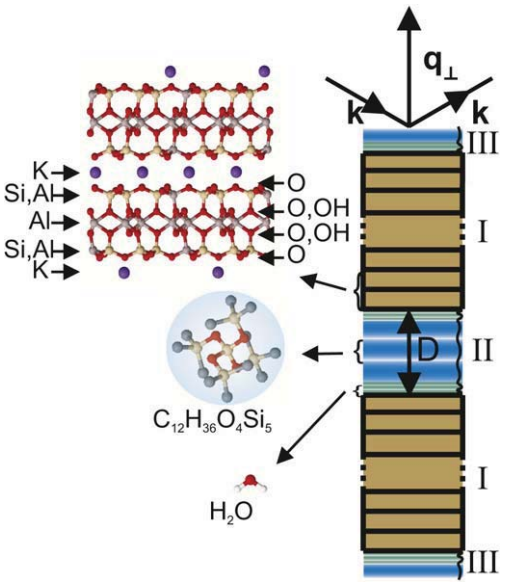

Figure 3. Schematic of the x-ray reflectivity geometry. Left-hand side: molecular structures of muscovite mica, tetrakis(trimethyl)siloxysilane (TTMSS) and water. The gap width D is defined as the distance between the surface potassium ions of the opposing mica crystals. Right-hand side: the roman numbers indicate the different regions contributing to the total structure factor: I mica, II confined liquid and III condensed liquid on the outer mica surfaces.

brought to identical lateral sizes through slow actuator motion. Consecutive equilibrium film thicknesses, which differ by one molecular layer of TTMSS are subtracted from one another, leading to step size values Δs as shown in figure 2(b).

2.3. Synchrotron x-ray reflectivity

The x-ray scattering geometry for the pair of free-standing mica membranes is shown in figure 1(b). The XRR experiments were performed at the coherent small angle x-ray scattering beamline X12SA (cSAXS) of the Swiss Light Source at the Paul Scherrer Institut. Experiments were carried out in two different XRR-setups. In both setups the specularly reflected intensities were measured as a function of perpendicular momentum transfer $q_\perp$ using a single-photon-counting 2D detector (PILATUS 100 K (Kraft *et al* 2009), pixel size 172 × 172 μm^2). The detector was positioned for XRR-setup 1 at 0.46 m and for XRR-setup 2 at 2.10 m behind the confinement device. For XRR-setup 2 a helium-filled flight tube was positioned in between the detector and the confinement device in order to avoid air scattering. Photon wavelengths of 0.75 Å and 0.67 Å (16.5 and 18.6 keV) were selected for XRR-setups 1 and 2, respectively. The high energies were chosen in order to reduce radiation damage of the liquid. The beam was focused onto the centre of the flat liquid thin films (focus sizes $H \times V$ of 147×10 and 80×5 μm^2, respectively). The perpendicular momentum transfer $q_\perp$ was scanned by tilting the confinement device over an angle θ with respect to the incoming beam direction. The scattered intensity was integrated at the position of the specular reflection at angle 2θ and an intrinsic average background intensity measured next to the reflection was subtracted.

The integrated intensity as a function of momentum transfer $I(q_\perp) = C|F(q_\perp)|^2$ is proportional to the squared modulus of the total structure factor $F(q_\perp)$. C is an angle-dependent proportionality factor, which accounts for the illuminated area, the illumination time, the polarization of the x-ray beam and the Lorentz factor (Vlieg 1997). We express $F = F_\mathrm{I} + F_\mathrm{II} + F_\mathrm{III}$ (Perret *et al* 2010) as a sum of structure factors arising from individual regions of the confinement arrangement, with F_I being from mica, F_II from the confined liquid and F_III from liquid condensed on the outer mica surfaces (figure 3).

The total integrated intensity (Perret *et al* 2010) is given by

$$I(q_\perp) = C(|F_\mathrm{I}|^2 + |F_\mathrm{II}|^2 + |F_\mathrm{III}|^2 + 2\,\mathrm{Re}[F_\mathrm{II}F_\mathrm{I}^*] + 2\,\mathrm{Re}[F_\mathrm{III}F_\mathrm{I}^*]), \quad (1)$$

where Re stands for the real part and the rapidly oscillating interference term $\mathrm{Re}[F_\mathrm{II}F_\mathrm{III}^*]$ vanishes since it cannot be resolved by the detector (Perret *et al* 2010). F_I is calculated from the known crystal structure of mica (Güven 1971), while F_II and F_III are modelled assuming Gaussian electron density profiles for the liquid layers (Perret *et al* 2010). The number of peaks and their height, width and position are determined in fits of various model structure factor amplitudes, $|F_\mathrm{calc}|$, to the measured ones, $|F_\mathrm{meas}|$, using a logarithmic least-squares minimization procedure (Hirano *et al* 1998). The fitting procedure has proven to be highly sensitive to individual fitting parameters (Perret *et al* 2009).

3. Results and discussion

Interferometric measurements of layering transitions in TTMSS confined by supported and free-standing mica membranes are presented and compared with each other. The findings are correlated with density profiles obtained from XRR data for five film thicknesses.

3.1. Layering transitions for supported mica membranes

Surface forces as a function of the film thickness D were measured for TTMSS confined by four different pairs of silica-supported mica membranes of different thicknesses ranging from 2.3 to 3.5 μm. The measured force curves exhibit oscillatory features as shown in figure 4(a). The surfaces approached each other at a constant actuator speed of 1 nm s^{-1} and were separated again with 2 nm s^{-1} after each layering transition in order to measure all attractive minima of the oscillatory force profile. In figure 4(a), the force F has been normalized by the mean mica radius of curvature R because this quantity is proportional to the interaction free energy between two flat surfaces (Derjaguin 1934). The radius of curvature ($R = 21.6$ mm) was determined from lateral scans of the spectrometer with the mica membranes being separated. Repulsive forces (positive) occurred at film thicknesses D below 7 nm. Note that D may be offset by an unknown amount due to water adsorbed onto the mica surfaces (Malani and

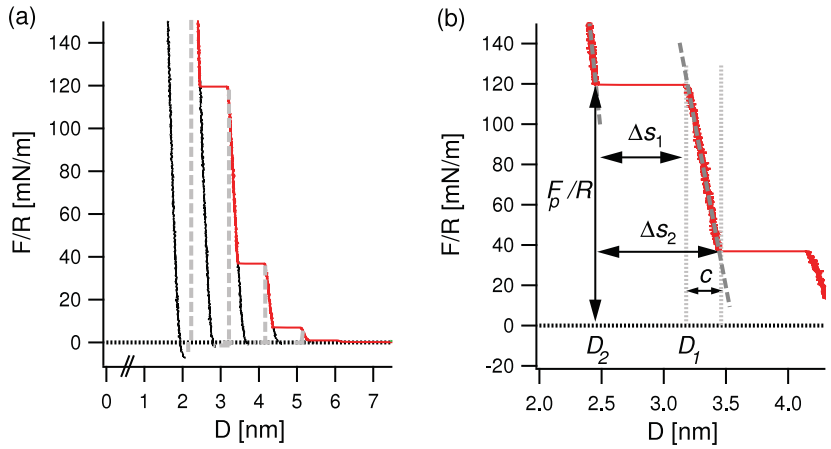

Figure 4. Oscillatory force profile for confined TTMSS. (a) Example of an oscillatory force curve measured with silica-supported mica. The normalized force F/R is plotted against the film thickness D. The red parts of the curves were obtained during approach, the black parts during retraction of the surfaces. Dashed grey lines indicate parts of the oscillatory force profile which are not measurable by means of this method. (b) Close-up of two successive layering transitions, showing the definitions of step size and compression used in our analysis.

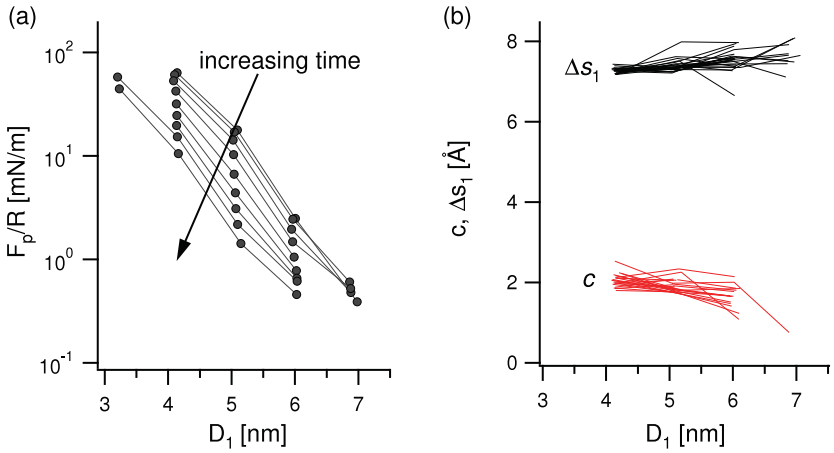

Figure 5. Measurement on compressed liquid films. (a) Normalized peak force as a function of pre-transition film thickness D_1 (before layering transition) for subsequent compression cycles on a pair of mica membranes of thickness 2.342 μm. (b) Measured compression c and step size Δs_1 for layering transitions in subsequent compression cycles for this mica pair.

Ayappa 2009, Christenson 1993, Balmer *et al* 2008). With increasing normal force up to six layering transitions were observed. A close-up of two successive layering transitions is shown in figure 4(b). Following a layering transition, the film is compressible by the amount c to the distance D_1 at which a next transition occurs and distance D_2 is reached. For each layering transition we have determined the values of the compression c, the step sizes Δs_1 and $\Delta s_2 = \Delta s_1 + c$ and the corresponding peak force F_p. Figure 5 summarizes the results for a series of compression cycles on one of the four membrane pairs.

The peak forces (figure 5(a)) are observed to increase exponentially with decreasing film thickness and to decrease continuously with time (over 2 days). Long-term decreasing forces may be related to the uptake of water or other slow changes at the solid–liquid interface. It is interesting to note that the film thicknesses at which the transitions occur remain fairly constant as indicated by the dots. The compression c increases slightly after each transition (figure 5(b)).

The constant step size Δs_1 suggests that the transition uses a constant vertical space for reordering the system. The step size $\overline{\Delta s_1}$, averaged over four data sets from different compression cycles, equals 7.5 ± 0.3 Å. The average peak to peak distance $\overline{\Delta s_2}$ including an average compression of $\bar{c} = 2.0 \pm 0.6$ Å equals 9.5±1.1 Å, which is slightly larger than the molecular diameter 9.0 Å (Yu *et al* 2000). This distance is usually interpreted to be equal to the layer spacings.

3.2. Layering transitions for free-standing mica membranes

Film thickness transitions were studied on eight different pairs of free-standing mica membranes having a thickness ranging from 1.8 to 5.1 μm. For each pair, series of confined films of different thicknesses were produced and step size values associated with layering transitions were obtained following the two methods explained in section 2.2. Layering transitions were investigated by both measuring the change in film thickness Δs upon film thickness transition

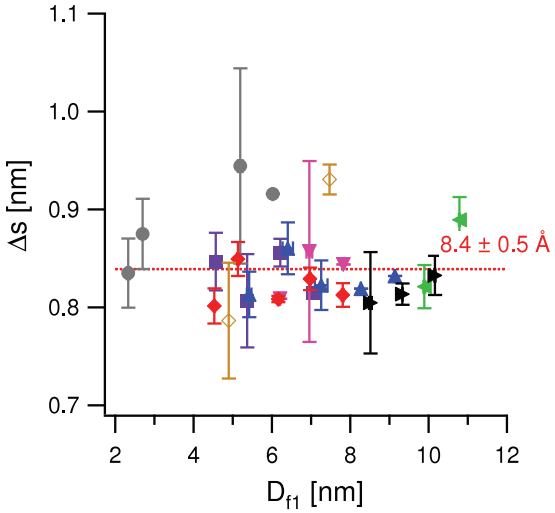

Figure 6. Measured average step sizes for equilibrated liquid films plotted versus initial film thickness for eight different data sets with mica thicknesses of ■ 4.933 μm, ● 4.363 μm, ▲ 5.151 μm, ▼ 1.832 μm, ◄ 3.623 μm, ► 3.464 μm, ♦ 3.636 μm, ◊ 4.303 μm. The error bars indicate the standard deviations. The overall step size average of 8.4 ± 0.5 Å is indicated by the dotted red line.

(figure 2(a)) and measuring the difference in film thickness Δs of subsequently equilibrated films (figure 2(b)). Both procedures revealed similar step sizes and are practically indistinguishable. Figure 6 shows the measured average step sizes Δs as a function of the pre-transition film thickness D_{f1} with corresponding standard deviations. The standard deviations for the measured film thicknesses were in average below 1 Å and are therefore not plotted.

The average step size $\overline{\Delta s}$ of 8.4 ± 0.5 Å is larger than the value of 7.5 ± 0.3 Å which was measured for the compressed liquids. Adding the compression to the latter step size value reveals an average step size of 9.5 Å for compressed liquids. This suggests that layering transitions liberate more space in the equilibrated liquid films for free-standing mica and that the films are less compressed.

3.3. Density profiles by x-ray reflectivity

XRR measurements were performed on five TTMSS films in equilibrium having different thicknesses up to 11 nm. The mica membranes used in XRR-setup 1 had a thickness of 5.612 μm and the ones in XRR-setup 2 had a thickness of 5.340 μm. The measured structure factor amplitudes are shown in figure 7(a) together with their best fits. The corresponding electron density profiles are shown in figure 7(b). They are broadened with the experimental resolution $1.1/q_{\perp,\max} = 0.8$ Å for XRR-setup 1 and 0.5 Å for XRR-setup 2 (Fenter 2002). The fitting procedure is sensitive to individual fitting parameters such as number of layers, layer spacings and average electron density (Perret *et al* 2009, 2010).

The best fit electron density profiles show a well defined, quasi-periodic, location of the Gaussian peaks across all films except for the film of largest thickness, where the profile resembles that of bulk liquid. Each peak represents the laterally averaged electron density of a molecular layer parallel to the confining walls. The layer adjacent to the confining mica surfaces, which we call *boundary layer*, shows a small peak for XRR-setup 1 and a broad peak of higher intensity, which overlaps with three distinct peaks for XRR-setup 2, see figure 8. This part of the profile can be attributed to adsorbed water layers on the hydrophilic mica surfaces for XRR-setup 1. We interpret the boundary layer density for XRR-setup 2 as a mixture of adsorbed water and TTMSS having a thickness of about a molecular monolayer of TTMSS (3 ML of water). Note that the existence of the boundary layer is very clear since absence of such a boundary layer in the electron density would lead to significant deviations from the best fit (black dashed curves in figures 7(a) and (b), overlaid with the second data set from above). Table 1 summarizes for each of the three TTMSS films measured with XRR-setup 2 the structural parameters providing the best fit to the measured reflectivity curve. For the determination of the average electron density and the average layer spacings only the inner TTMSS layers (figure 8), i.e., without the boundary layer, were considered.

Table 1. Structural parameters providing the best fit. Error margins in a parameter are given for a deviation in the fit residual ΔErr (Perret *et al* 2009) of 0.01, keeping the other tabled parameters fixed.

D_{XRR} (nm)	9.46 ± 0.01	6.80 ± 0.01	4.39 ± 0.01
Number of TTMSS layers	9(+1)	7	4
Average layer spacing of inner TTMSS layers (Å)	11.0 ± 0.2	9.9 ± 0.1	10.3 ± 0.8
Distance between *a* and *b* (Å)[a]	9.0 ± 0.5	9.8 ± 0.1	10.4 ± 0.4
Electron density, percentage of bulk value (%)	100 ± 12	85 ± 7	79 ± 24
Number of fitting parameters	30	32	29
Fit residual Err (Perret *et al* 2009)	0.44	0.44	0.44

[a] Length of bars in figure 7(b).

From the parameters in table 1 the following conclusions are drawn.

(i) The average layer spacings are larger than the molecular diameter of 9.0 Å (Yu *et al* 2000) and the measured step sizes Δs as measured by white light interferometry for both, equilibrated and compressed films. The former may be attributable to enhanced out-of-plane fluctuations (Mittal *et al* 2008) and the latter further supports the idea that layering transitions are reordering the entire system.

(ii) For XRR-setup 2, the layer spacings between the boundary layer and the outmost inner layer increases for decreasing film thickness (see black bars in figure 7). This trend may explain why the step size Δs is smaller than the layer spacings. The measurements with XRR-setup 1 do not fit within this trend, because less water was adsorbed.

(iii) The electron density is lower than the bulk electron density and shows a decreasing trend towards smaller film thicknesses for both XRR-setups. However, as can be seen from the error margins, the fits are less sensitive to the average electron density.

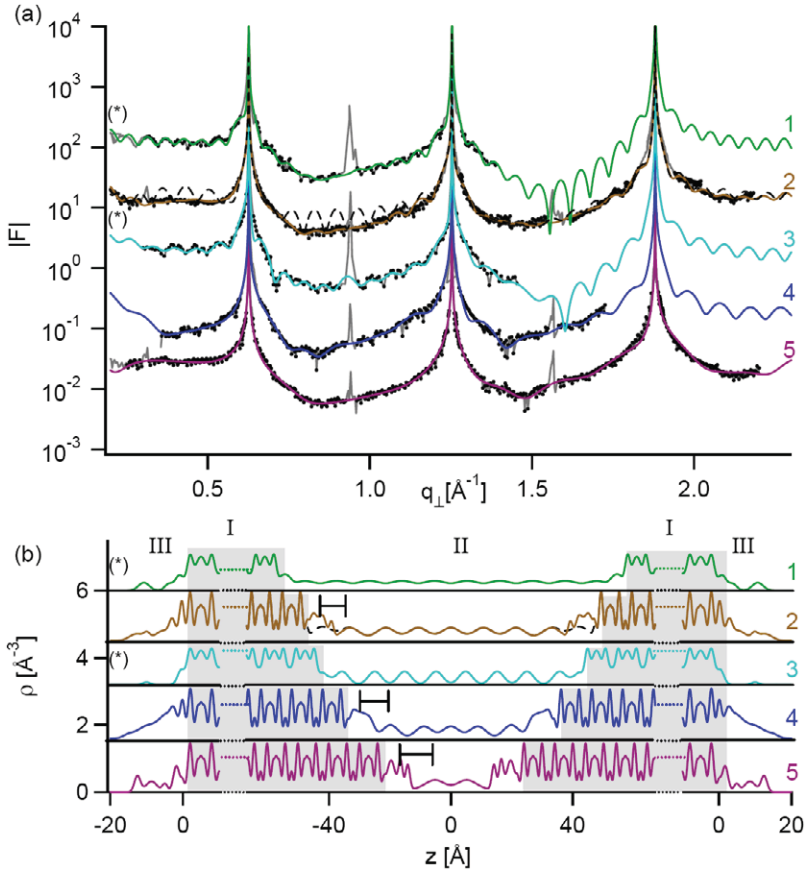

Figure 7. Measured and calculated best fit structure factor amplitudes with corresponding electron density profiles. (a) Measured structure factor amplitudes (grey curve, grey dots for fitted data points) and calculated structure factors (coloured curves) for five different film thicknesses. The structure factor amplitudes measured with XRR-setup 1 are indicated by an asterisk (∗). The other structure factor amplitudes were measured with XRR-setup 2. (b) Corresponding electron density profiles, with different regions of the confinement device indicated by roman numbers as in figure 3: I mica (grey shaded area), II confined liquid and III liquid on the outer mica membranes. Black bars indicate the distance between the boundary layer and the outmost inner layer in the film. The profiles are vertically offset for better readability.

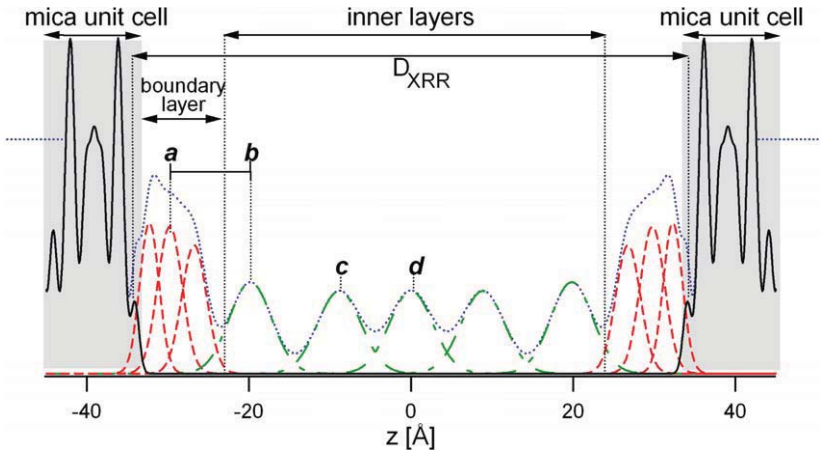

Figure 8. Schematic of the liquid density profile. Overall density profile (blue dotted curve), individual Gaussian peaks of inner TTMSS layers (green dashed-dotted curve), three peaks (mixed water/TTMSS) attributed to the boundary layer (red dashed curve) and mica density (black curve). D_{XRR} is the distance between the surface potassium layers.

(iv) The inner TTMSS seems to become more diffusely layered towards larger film thicknesses. This may be due to larger out-of-plane thermal fluctuations.

(v) The film thicknesses D_{XRR} are in good agreement with the optical film thickness transition measurements; the differences between the film thicknesses are roughly a multiple of 8.4 ± 0.5 Å for both XRR-setups. The differences in film thicknesses are directly related to the difference in number of layers. Considering XRR-setup 2, the transition from 6.8 to 4.4 nm in film thickness with

a step of 2.4 nm is a layering transition of three layers. This number agrees with the determined difference in the number of density peaks (from 7 to 4). If one considers the difference between the larger film thickness 9.5 and 6.8 nm, which is 2.7 nm, one would also expect a layering transition of three layers. The structure factor of the large film can be fitted with 9 or 10 layers, with only a small difference in logarithmic residual (ΔErr $\approx$ 0.01, (Perret *et al* 2009)). Yet, the resulting layer spacings between the boundary and the outmost inner layers are for both fits the same. We emphasize that the strength of the fitting model lies in determining the out-of-plane structure for small film thicknesses ($D < 8$ nm).

4. Conclusion and outlook

We have demonstrated that the combination of x-ray reflectivity and optical interferometry is ideal to gain a better understanding of confinement-induced ordering effects. The out-of-plane layered structure (i.e. electron density profile) of a molecular liquid confined between two free-standing mica membranes was directly determined by XRR experiments at the cSAXS beamline. We have chosen TTMSS as a model fluid since it enables us to directly compare XRR and surface force experiments on the same system. Notably, it was found that the layer spacing in the confined liquid is larger than what was expected from film thickness transition and force measurements in the eSFA. This finding suggests that film thickness transitions represent a complete reordering of the confined film rather than a simple expulsion of a molecular layer. Furthermore, at least one boundary layer adjacent to the confining mica walls was identified. These boundary layers were found to exhibit an electron density and periodicity significantly different from the inner layered structure. In the future, the structure of other important liquids under nanometre confinement, e.g., water, is to be determined by non-specular x-ray reflectivity.

Acknowledgments

We thank the staff of the cSAXS beamline for assistance. This work was supported by the Swiss National Science Foundation.

References

Als-Nielsen J and McMorrow D 2001 *Elements of Modern X-ray Physics* (New York: Wiley)
Ayappa K G and Mishra R K 2007 *J. Phys. Chem.* B **111** 14299
Balmer T E 2007 Resolving structural and dynamical properties in nano-confined fluids *PhD Thesis* Diss. ETH No. 17359
Balmer T E, Christenson H K, Spencer N D and Heuberger M 2008 *Langmuir* **24** 1566
Born M and Wolf E 1980 *Principles of Optics* (Oxford: Pergamon)
Christenson H K 1983 *J. Chem. Phys.* **78** 6906
Christenson H K 1993 *J. Phys. Chem.* **97** 12034
Clarkson M T 1989 *J. Phys. D: Appl. Phys.* **22** 475
Derjaguin B 1934 *Kolloid-Z.* **69** 155
Diaz A, David C, Guo H, Keymeulen H, Pfeiffer F, Wegdam G, Weitkamp T and van der Veen J F 2005 *Physica* B **357** 199
Diaz A and van der Veen J F 2007 *Thin Solid Films* **515** 5645
Fenter P A 2002 Applications of synchrotron radiation in low-temperature geochemistry and environmental sciences *Rev. Mineral. Geochem.* **49** 149
Golan Y, Seitz M, Luo C, Martin-Herranz A, Yasa M, Li Y L, Safinya C R and Israelachvili J 2002 *Rev. Sci. Instrum.* **73** 2486
Güven N 1971 *Z. Kristallogr.* **134** 196
Heuberger M 2001 *Rev. Sci. Instrum.* **72** 1700
Heuberger M, Vanicek J and Zäch M 2001 *Rev. Sci. Instrum.* **72** 3556
Heuberger M and Zäch M 2003 *Langmuir* **19** 1943
Hirano T, Usami K, Ueda K and Hoshiya H 1998 *J. Synchrotron Radiat.* **5** 969
Horn R G and Israelachvili J N 1980 *Chem. Phys. Lett.* **71** 192
Horn R G and Israelachvili J N 1981 *J. Chem. Phys.* **75** 1400
Idziak S H J, Koltover I, Davidson P, Ruths M, Li Y L, Israelachvili J N and Safinya C R 1996a *Physica* B **221** 289
Idziak S H J, Koltover I, Israelachvili J N and Safinya C R 1996b *Phys. Rev. Lett.* **76** 1477
Idziak S H J, Koltover I, Liang K S, Israelachvili J N and Safinya C R 1995 *Int. J. Thermophys.* **16** 299
Kjellander R and Sarman S 1991 *J. Chem. Soc. Faraday Trans.* **87** 1869
Klein J and Kumacheva E 1998 *J. Chem. Phys.* **108** 6996
Kraft P, Bergamaschi A, Broennimann C, Dinapoli R, Eikenberry E F, Henrich B, Johnson I, Mozzanica A, Schleputz C M, Willmott P R and Schmitt B 2009 *J. Synchrotron Radiat.* **16** 368
Malani A and Ayappa K G 2009 *J. Phys. Chem.* B **113** 1058
Mittal J, Truskett T M, Errington J R and Hummer G 2008 *Phys. Rev. Lett.* **100** 145901
Nygård K, Satapathy D K, Buitenhuis J, Perret E, Bunk O, David C and van der Veen J F 2009 *Europhys. Lett.* **86** 66001
Nygård K, Satapathy D K, Bunk O, Diaz A, Perret E, Buitenhuis J, Pfeiffer F, David C and van der Veen J F 2008 *Opt. Express* **16** 20522
Perret E, Nygård K, Satapathy D K, Balmer T E, Bunk O, Heuberger M and van der Veen J F 2009 *Europhys. Lett.* **88** 36004
Perret E, Nygård K, Satapathy D K, Balmer T E, Bunk O, Heuberger M and van der Veen J F 2010 *J. Synchrotron Radiat.* at press
Satapathy D K, Bunk O, Jefimovs K, Nygård K, Guo H, Diaz A, Perret E, Pfeiffer F, David C, Wegdam G H and van der Veen J F 2008 *Phys. Rev. Lett.* **101** 136103
Satapathy D K, Nygård K, Bunk O, Jefimovs K, Perret E, Diaz A, Pfeiffer F, David C and van der Veen J F 2009 *Europhys. Lett.* **87** 34001
Seeck O H, Kim H, Lee D R, Shu D, Kaendler I D, Basu J K and Sinha S K 2002 *Europhys. Lett.* **60** 376
Snook I and Henderson D 1978 *J. Chem. Phys.* **68** 2134
Vlieg E 1997 *J. Appl. Crystallogr.* **30** 532
Wang J C and Fichthorn K A 2000 *J. Chem. Phys.* **112** 8252
Yu C J, Richter A G, Kmetko J, Datta A and Dutta P 2000 *Europhys. Lett.* **50** 487